IEEE Access
Multidisciplinary | Rapid Review | Open Access Journal

Received October 20, 2020, accepted October 23, 2020, date of publication October 27, 2020, date of current version November 12, 2020.

*Digital Object Identifier 10.1109/ACCESS.2020.3034120*

# Multiband Terahertz Self-Complementary Metasurface

**SE-MI KIM, (Associate Member, IEEE), CELSO M. LEITE, JU-YEONG PARK, HYO-JEONG KIM, AND JAE-HYUNG JANG, (Member, IEEE)**
School of Electrical Engineering and Computer Science, Gwangju Institute of Science and Technology, Gwangju 61005, South Korea

Corresponding author: Jae-Hyung Jang (jjang@gist.ac.kr)

This work was supported in part by the National Research Foundation of Korea (NRF) funded by the Korean Government (Ministry of Science, ICT, and Future Planning) under Grant 2017R1A2B3004049, and in part by Korea Electric Power Corporation under Grant R18XA06-79.

**ABSTRACT** A self-complementary metasurface is presented for application in multiband terahertz filters. The unit cell structures of the self-complementary metasurface consist of a combination of an ordinary Jerusalem cross and its complementary counterpart that resonates in the THz regime. The columnar repetition of ordinary and complementary resonator structures enables complementary spectral responses for incident waves with mutually orthogonal linear polarizations. The operating principles of the self-complementary metamaterial with the interaction between the juxtaposed ordinary and complementary Jerusalem crosses are explained using an equivalent circuit method and are confirmed with a full-wave electromagnetic simulation. The designed self-complementary metasurface functions as a selective bandstop filter (BSF) or bandpass filter (BPF) depending on the polarization states of the incident wave. The fabricated metasurface exhibits high polarization purity, exemplified by a polarization extinction ratio as high as 24 dB. The transmittance phases of the two orthogonally polarized waves have phase differences between $-73^\circ$ and $83^\circ$ within a broad frequency range.

**INDEX TERMS** Terahertz, metasurface, bandpass filter, bandstop filter, multiband.

## I. INTRODUCTION

Terahertz (THz) technology deals with electromagnetic waves with wavelengths between 3 mm and 30 $\mu$m. In recent years, terahertz technology has attracted considerable attention due to its potential applications [1], and the number of published reports on it has increased rapidly [2]. Due to their nonionizing low-energy characteristics as well as their high transmission through dielectric materials, THz waves have the benefit of being able to penetrate visually opaque materials while being harmless to the human body. Thus, these waves are used in applications such as biosensing [3], imaging [4] and material characterization [5]. With the growth of wireless data traffic, the THz frequency band can be a promising candidate for supporting future ultrabroadband communications, bridging the gap between millimeter wave (mm-wave) and optical frequency ranges [6]. THz communications for short-range wireless links [7] and satellite links [8] have been reported. Moreover, spectrum regulations and ongoing standardization activities have been presented in the field of THz communications [9].

However, further development of the technology is still hindered by a lack of devices that can effectively control and manipulate THz waves, such as modulators, filters and polarizers. THz active and passive components are still under development to make it possible for THz technology to penetrate niche industrial applications [10].

Metamaterials play an important role in active and passive device design due to their versatility in being able to be tailored for desired functionalities in a broad spectral range from the microwave region to the visible region [11]. Metamaterials have also had a profound impact on advances in THz science and technology by realizing appropriate spectral responses in the THz frequency band [12].

Various metamaterial designs have been reported to demonstrate THz devices, such as absorbers, polarization converters, quarter wave plates, and filters. A six-band terahertz metamaterial absorber was presented [13], and alignment-insensitive THz absorbers were demonstrated by using a bilayer metasurface [14]. A multiple reflection and

The associate editor coordinating the review of this manuscript and approving it for publication was Shah Nawaz Burokur.

interference model of a metamaterial was developed to guide the design of THz absorbers [15]. Metamaterials were also utilized to control the polarization of incident waves. A nondispersive cross polarization converter structure converts linearly polarized waves to cross-polarized waves [16]. A trilayered chiral metasurface was proposed for linear polarization conversion [17]. A metasurface antenna with wide-gain-bandwidth was reported to demonstrate high-efficiency THz radiation [18]. A THz quarter-wave plate was demonstrated with an anisotropic metasurface [19]. To electrically control THz wave transmission, metamaterial-based amplitude modulators were realized on top of GaAs [20], [21] and GaN electron device platforms [22].

Most of the metamaterials operating at THz frequencies consist of metallic resonators arrayed on top of electromagnetically transparent substrates. Ordinary metamaterials are composed of unit cell structures that are electrically isolated resonators, while complementary metamaterials have negative metallic images of ordinary metamaterials. They exhibit complementary spectral responses. The most common unit cell structures are based on split-ring resonators (SRRs) and the complementary SRR (CSRR), and they exhibit bandstop filter (BSF) and bandpass filter (BPF) responses, respectively [23]. A CSRR-based BPF using a lossy glass substrate was reported with a high spurious band rejection ratio [24]. Nested SRR (NeSRR) structures where a smaller SRR was nested in a larger SRR were realized on a flexible material [25] and a quartz substrate with subwavelength structures (SWSs) [26].

Another way to realize a THz filter is to utilize the interference in a multilayer structure. A BSF was demonstrated using a stack of several ultrathin silicon wafers and air gaps with a proper index arrangement [27]. A cascaded bilayer metasurface demonstrated antireflection structures with a narrow band filter response [28]. A multilayer BPF was implemented using a wire-and-plate structure on benzocyclobutene (BCB) films [29]. Pairs of metallic crosses were located on both sides of the complementary cross structure, and all were embedded in a dielectric bar to decrease the reflection loss [30].

Various unit cell designs have been proposed to realize multiband spectral characteristics. Symmetric SRRs with different sizes have been utilized to achieve two distinct electric resonances as a step towards broadband THz devices [31]. Polarization-insensitive filter characteristics were realized using a metasurface consisting of symmetric cross pillars [32]. Multiple-resonance excitation was realized in a composite metamaterial for ultrawide BPFs [33]. Tunable filters and polarization rotators were also realized using vanadium oxide ($VO_2$). The operational characteristics of the device were tuned by the temperature-sensitive electrical conductivity of $VO_2$ [34], [35].

The above described filters exhibit either bandpass or bandstop frequency responses. For cases where only one response type is required, a filter with polarization-insensitive characteristics may be preferred because of easy alignment. From the point of view of functionality, it may be beneficial to have a filter capable of offering bandpass and bandstop responses at the same frequency band.

This paper reports a multiband THz filter based on a self-complementary metasurface. A self-complementary metamaterial consists of an ordinary resonator and its complementary counterpart placed side by side. For the one linear polarized incident wave, a self-complementary metasurface operates as a BSF while showing a BPF response for the other orthogonally polarized incident wave. The characteristics of a self-complementary metamaterial make it possible to design a 2-in-1 filter, whose response can be easily switched between a BSF and a BPF by mechanically rotating the device by 90°. In a GHz frequency range, simulation studies of a self-complementary metasurface consisting of an SRR and a CSRR have been reported [36], and similar structures were experimentally realized [37]. A self-complementary metasurface consisting of rectangular patches and holes was reported for a polarization conversion [38]. Even though these devices showed BSF/BPF spectral responses depending on the incident polarization, their polarization extinction ratio (PER) performance have large room to improve because their resonance frequencies were different for the two orthogonal polarizations or their band rejection properties are not good.

In this paper, the proposed multi-band THz metasurface exhibits the well matched resonance frequencies for x- and y-polarization in the triple THz frequencies so that the polarization rejection properties are much better than those of other reported self-complimentary metasurfaces. The operating principles and design guidelines of this THz multiband self-complementary metasurface are presented using electromagnetic simulation and an equivalent circuit method, and their performance is experimentally verified.

## II. DESIGN AND EQUIVALENT CIRCUIT REPRESENTATION

The metasurface chosen to realize the THz filter in this work is based on a self-complementary Jerusalem cross structure. The Jerusalem-cross shape has been used for other applications, such as a quasi-optical diplexer [39], a THz absorber [40] and frequency-selective surfaces (FSSs) [41]. The unit cell in this metasurface consists of a metallic Jerusalem cross and its complementary counterpart. The schematic of the unit cell is shown in Fig. 1.

Rotational symmetric metasurfaces exhibit the same frequency response for the incident x- and y-polarizations, so they can be described by the same equivalent circuit for both incident polarizations. The gap between the metal acts like a capacitor, and the metal line acts like an inductor. An ordinary metasurface, consisting of periodically arranged isolated metallic resonators, resembles a light field metal mask on a quartz substrate and can be analyzed by a serial LC resonator [42], [43] with a bandstop frequency response. On the other hand, a complementary metasurface, which has a negative image of the ordinary metasurface, operates like a parallel LC resonator [44] with a bandpass frequency response. A self-complementary metasurface exhibits an

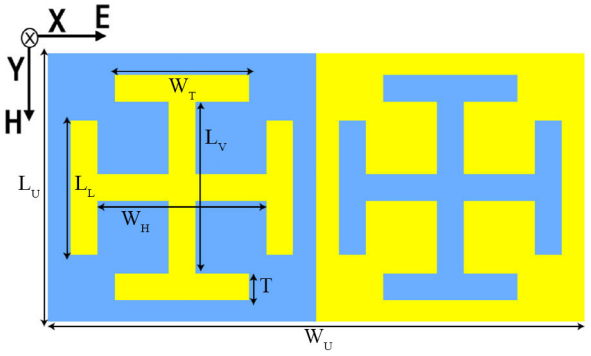


**FIGURE 1.** Self-complementary metasurface unit cell using a Jerusalem cross design. ($W_T = L_L = 25\ \mu m$, $W_H = L_V = 35\ \mu m$, $T = 5\ \mu m$, $L_V = 50\ \mu m$, $W_U = 100\ \mu m$).

anisotropic structure, and its response depends on the polarization of the incident wave. Therefore, it has a polarization-dependent spectral response, and it should be represented by two distinct equivalent circuits depending on the incident polarizations.

Fig. 2 and 3 show the simplified equivalent circuits of the self-complementary metasurface for x- and y-polarization, respectively. The substrate effect considered in the equivalent circuit presented in [45] is neglected in the equivalent circuits to derive an analytic expression of the reactance and to determine the resonance frequencies in closed form. The gap between the loading ends acts as a capacitor, and the metal line of the cross acts as an inductor. The series connected $L_S$ and $C_S$ are from the equivalent circuit of the ordinary metasurface, while the parallel connected $L_P$ and $C_P$ are from the equivalent circuit of the complementary metasurface.

To examine the response to the x-polarized incident wave, the equivalent circuit shown in Fig. 2(b) was analyzed. The reactance $X_1$ of the circuit is

$$X_1(\omega) = \frac{-\omega^4 L_P^2 C_P^2 xy + \omega^2 L_P C_P (xy + y + 1) - 1}{\omega C_S (1 - \omega^2 L_P C_P)} \quad (1)$$

where $x = L_S/L_P$, $y = C_S/C_P$. At the low frequency limit, $X_1(\omega) \to -\infty$ when $\omega \to 0$, implying that the circuit acts as an open circuit where the signal is transmitted. In a similar way, the circuit acts as an open circuit, $X_1(\omega) \to \infty$ when $\omega \to \infty$ at the high frequency limit. When $X_1(\omega) = 0$, the circuit operates as a short circuit that allows no transmission; then, the frequency satisfying this condition is given by

$$\omega_{1,3} = \sqrt{\frac{(xy + y + 1) \pm \sqrt{(xy + y + 1)^2 - 4xy}}{2L_S C_S}} \quad (2)$$

By solving for the open-circuited case, $X_1(\omega) \to \infty$, the frequency, where the transmission is high, is found to be

$$\omega_2 = \frac{1}{\sqrt{L_P C_P}} \quad (3)$$

When $x = y = 1$, $\omega_2$ is determined to be the geometric mean of $\omega_1$ and $\omega_3$ so that $\omega_2 = (\omega_1 \omega_3)^{1/2}$.

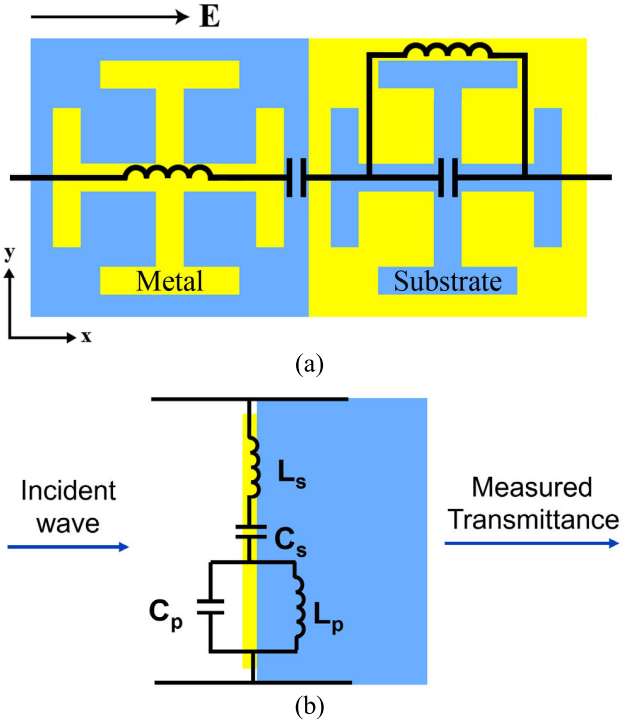


**FIGURE 2.** Equivalent circuit of the self-complementary metasurface for the x-polarized wave in the (a) plane view and (b) side view.

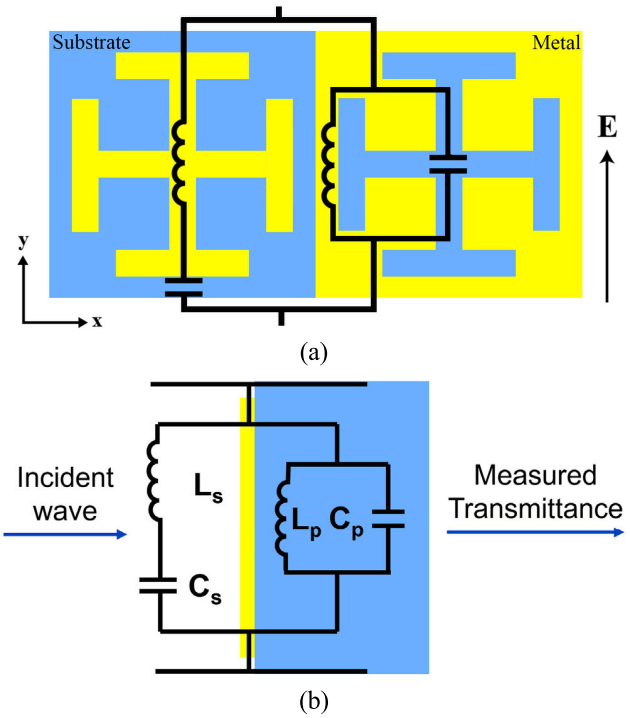


**FIGURE 3.** Equivalent circuit of the self-complementary metasurface for the y-polarized wave in the (a) plane view and (b) side view.

For the y-polarized incident wave, the reactance of the circuit represented in Fig. 3(b) can be represented by (4).

$$X_2(\omega) = \frac{\omega L_P (1 - \omega^2 L_S C_S)}{\omega^4 L_P^2 C_P^2 xy - \omega^2 L_P C_P (xy + y + 1) + 1} \quad (4)$$

This circuit acts as a short circuit at the low and high frequency limits, ($X_2(\omega \to 0) = 0$ and $X_2(\omega \to \infty) = 0$), exhibiting low transmission. The frequencies satisfying $X_2(\omega) \to \infty$, where the circuit exhibits high transmission, exactly matches the solutions of $X_1(\omega) = 0$, which are $\omega_1$ and $\omega_3$ represented by (2). By solving $X_2(\omega) = 0$ for the short circuit, the frequency where the transmission is low is

$$\omega_2 = \frac{1}{\sqrt{L_S C_S}} \tag{5}$$

When the condition of $xy = 1$ ($L_S C_S = L_P C_P$) is satisfied, the values of $\omega_2$ for both the x- and y-polarizations are identical. This analysis clearly shows that the equivalent circuits exhibit complementary responses for x- and y-polarized incident waves, and their resonant frequencies exactly match.

The reactance and complementary filter responses obtained from the equivalent circuit analysis are shown in Fig. 4. The device exhibits a BSF response for the x-polarized incident wave, while it shows a bandpass response for the y-polarized wave.

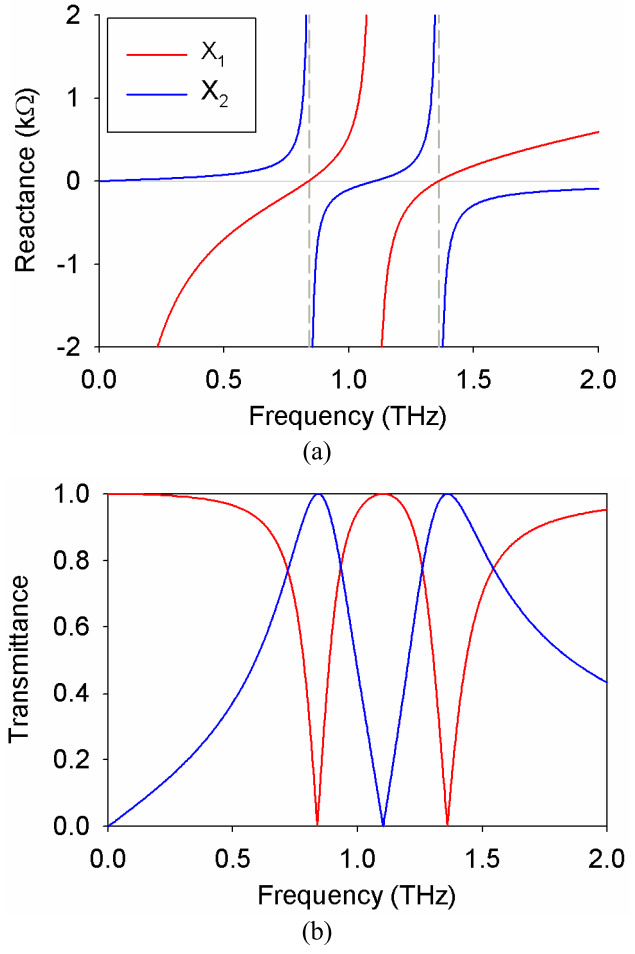


**FIGURE 4.** (a) Reactance and (b) filter responses obtained by the equivalent circuit analysis for x-polarization (red line) and y-polarization (blue line).

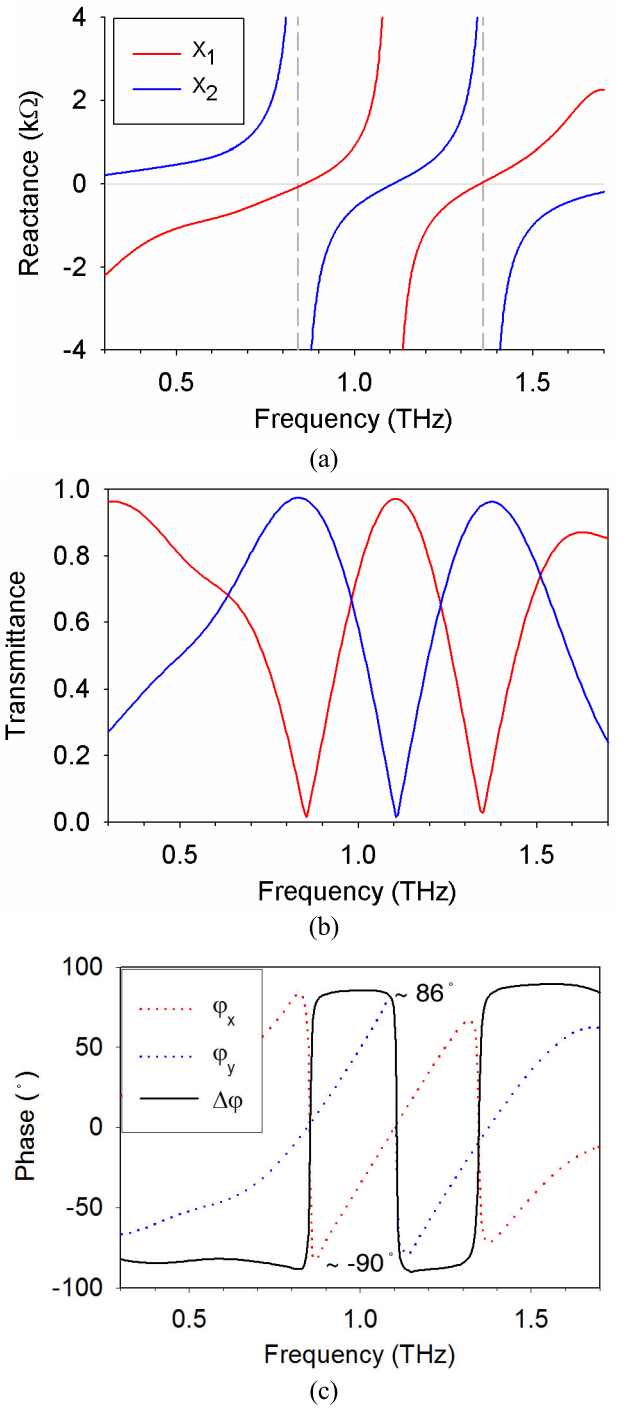


**FIGURE 5.** Simulation results of the self-complementary metasurface whose dimensions are shown in Fig. 1. (red line: x-polarization, blue line: y-polarization) (a) reactance, (b) transmittance, (c) phase response.

It is noteworthy that the self-complementary metasurface consisting of juxtaposed ordinary and complementary resonators can realize complementary spectral responses for the two orthogonal polarizations along with the two optical axes of the metasurface. It can achieve BPF for BSF responses with high polarization extinction ratios at multiple frequency bands owing to the complementary responses.

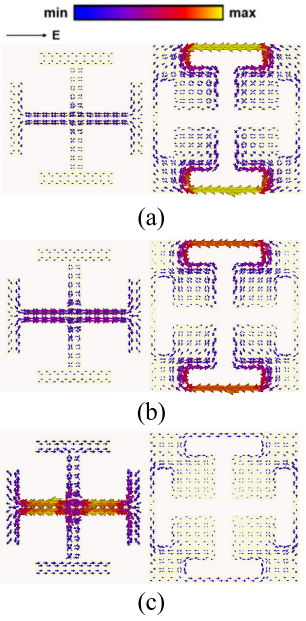


**FIGURE 6.** Surface current distribution for x-polarization at frequencies of (a) 0.85 THz, (b) 1.10 THz, and (c) 1.35 THz.

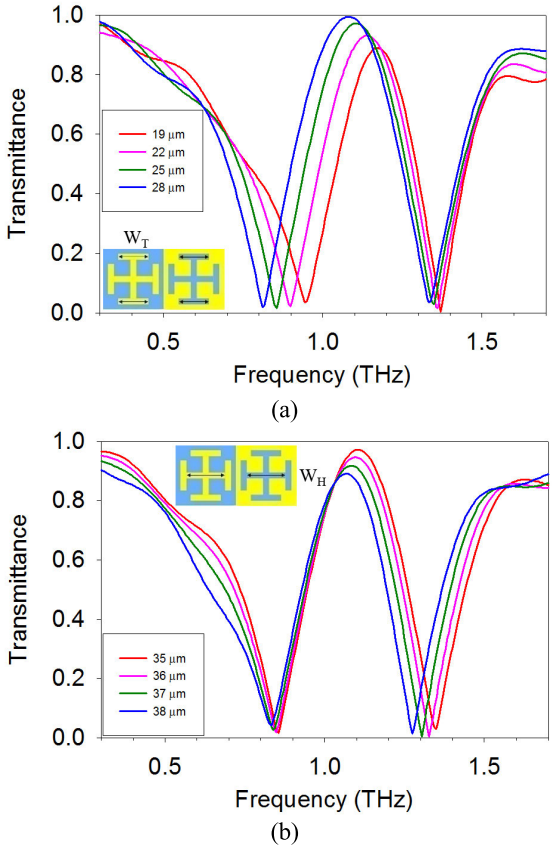


**FIGURE 7.** Transmittance for x-polarization depending on (a) top/bottom loading end widths and (b) horizontal cross widths.

## III. SIMULATION AND CHARACTERIZATION

The operational principles of the self-complementary metasurface are understood by using the equivalent circuit method.

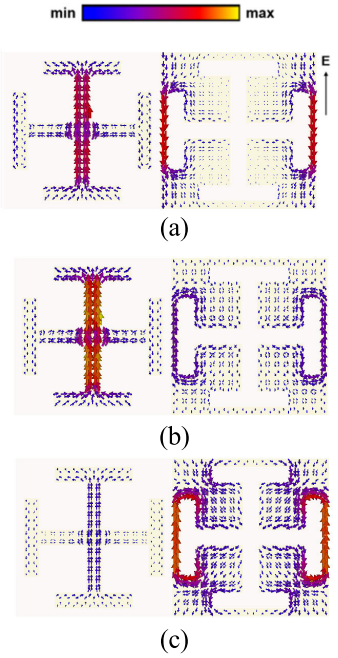


**FIGURE 8.** Surface current distribution for y-polarization at frequencies of (a) 0.83 THz, (b) 1.10 THz, and (c) 1.37 THz.

However, the detailed design should be carried out using an electromagnetic simulation method. The response of the proposed device was simulated using a commercial electromagnetic (EM) simulation tool. A linearized plane wave was adopted as the wave source, and periodic boundary conditions were applied to the unit cell to account for the device consisting of an array of hundreds of unit cells. The 300-$\mu$m-thick quartz substrate and Ti/Au (20/300 nm) metal were used for the metasurface. The Drude model was utilized to consider the material properties of gold [46].

Fig. 5(a) and (b) show the electromagnetically simulated reactance and the transmittance of the Jerusalem-cross-shaped self-complementary metasurface, whose dimensional parameters are shown in Fig. 1. When the calculation results obtained by the equivalent circuit method and EM simulation are compared, they match quite well. The electromagnetically simulated reactance of the metasurface exhibits essentially the same behavior as the result calculated with the equivalent circuit shown in Fig. 4(a). This result implies that the equivalent circuits shown in Fig. 2(a) and Fig. 3(a) are valid and can provide insight into how the self-complementary metasurface operates by visualizing the interaction between the ordinary and complementary resonator structures.

As expected from the analysis of the equivalent circuits shown in Fig. 4, the spectral responses in Fig. 5(b) show the BSF and BPF responses for the x- and y-polarized incident waves, respectively. For the x-polarized wave, the designed structure shows a multiband response with resonance peaks at 0.85, 1.10 and 1.35 THz. For the y-polarized wave, resonance peaks were observed at 0.83, 1.10 and 1.37 THz.

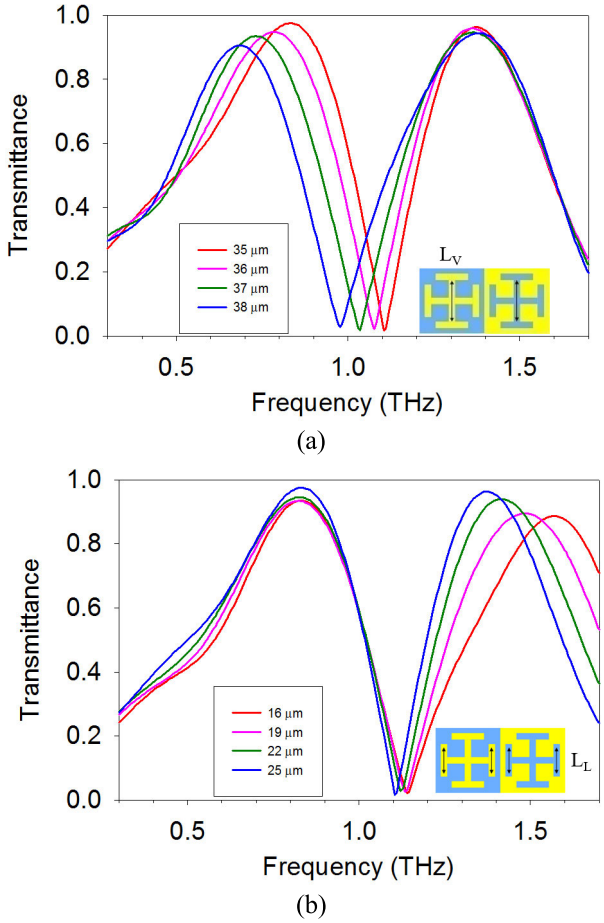


**FIGURE 9.** Transmittance for y-polarization depending on (a) vertical cross lengths and (b) left/right loading end lengths.

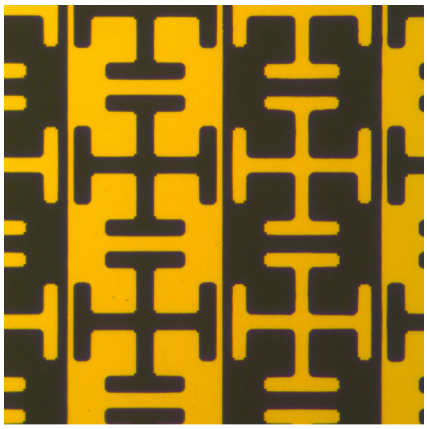

**FIGURE 10.** Optical image of fabricated self-complementary metasurfaces using the Jerusalem cross design.

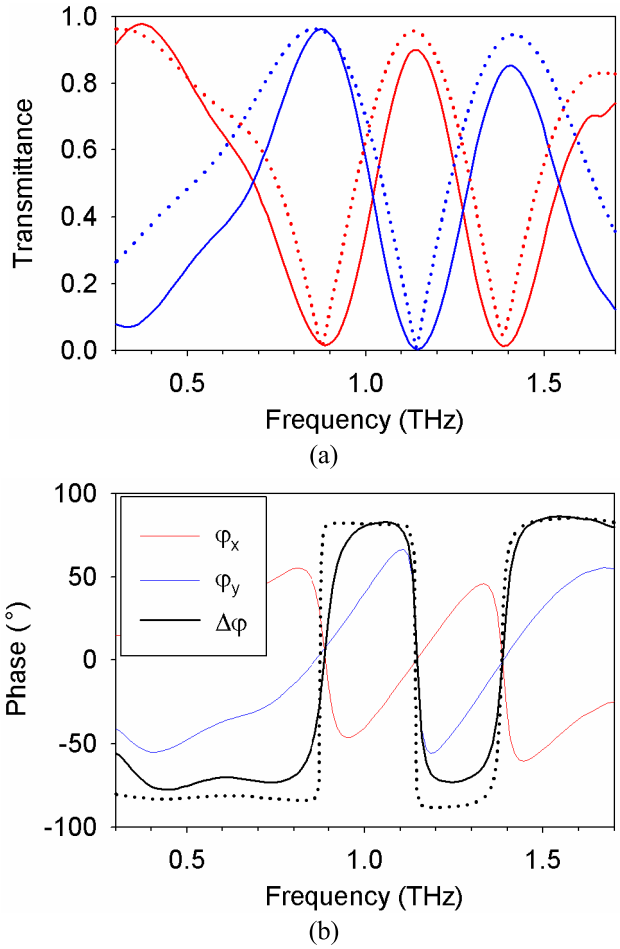


**FIGURE 11.** Measurement and simulation results (dotted line: simulation of the metasurface with a rounded corner, solid line: measurement) (a) transmittance (red line: x-polarization, blue line: y-polarization), (b) phase difference.

Fig. 5(c) shows the phase response for the two orthogonally polarized waves. The differential phase response, $\Delta\varphi$, is approximately $-90°$ or $86°$ within a broad frequency range.

By analyzing the surface current, the most dominant structural parameters that determine the resonance frequencies can be found for $\omega_1$, $\omega_2$ and $\omega_3$. Fig. 6 shows the surface current distributions for the $x$-polarized incident wave. At 0.85 and 1.10 THz, the surface current is mainly concentrated between the top and bottom loading ends of the complementary resonator, as shown in Fig. 6(a) and (b). This result exemplifies that $\omega_1$ and $\omega_2$ can be controlled by changing the width of the top and bottom loading ends, $W_T$, as shown in Fig. 7(a). At the third resonance frequency of 1.35 THz, a strong resonating surface current is observed at the horizontal element of the ordinary Jerusalem cross, as shown in Fig. 6(c), which implies that $\omega_3$ can be tuned by changing the width of the horizontal element of the cross, $W_H$. This possibility is confirmed by the parametric study given in Fig. 7(b).

The same parametric EM simulation studies were carried out for the y-polarized incident wave. The dominant geometric parameters that determine $\omega_1$, $\omega_2$ and $\omega_3$ for the y-polarized wave can be identified from the surface current distribution represented in Fig. 8. The surface current is concentrated in the vertical element at 0.83 THz and 1.10 THz, as shown in Fig. 8(a) and (b). Fig. 9(a) verifies that $\omega_1$ and $\omega_2$ can be controlled by adjusting the length of the vertical

**TABLE 1. Performance summary and comparison with the previously reported self-complementary metasurface.**

| Ref. | | This work | | | [36][a] | | | [37] | [38] |
|---|---|---|---|---|---|---|---|---|---|
| Operating frequency | x-polarization (GHz) | 890 | 1130 | 1380 | 2.13 | 2.15 | 3.27 | 4.59 | 5.1 |
| | y-polarization (GHz) | 870 | 1150 | 1410 | 2.13 | 2.15 | 3.01 | 4.64 | 5.4 |
| | Frequency mismatch (GHz) | 20 | 20 | 30 | 0 | 0 | 0.26 | 0.05 | 0.3 |
| | Percentile mismatch (%) | 2.3 | 1.8 | 2.1 | 0 | 0 | 8.6 | 1.1 | 5.6 |
| Band -width | $\Delta f_{3dB}$ (GHz) | 324 | 237 | 274 | 0.10 | 1.07 | 0.33[b] | 0.25[b] | 1.47[b] |
| | Fractional bandwidth (%) | 33 | 21 | 19 | 5 | 50 | 11[b] | 5[b] | 27[b] |
| Insertion loss(dB) | | 0.17 | 0.46 | 0.69 | 0.13 | 0.01 | 0.01[b] | 2.5[b] | 0.22[b] |
| Polarization extinction ratio (dB) | | 18 | 24 | 18 | 9 | 27 | 0.8[b] | 3[b] | 15[b] |
| Function | | BPF / BSF | | | | | | | Polarization converter |
| Unit cell structure | | Jerusalem cross / Complementary Jerusalem cross | | | SRR / C-SRR | | | SRR / C-SRR | Rectangular patch / hole |

[a]Simulation results only.
[b]Estimated value by using the graphs presented in the references.

bar, $L_V$, of the Jerusalem cross. On the other hand, a strong surface current flow is observed around the left/right loading ends of the complementary resonator at 1.37 THz, as shown in Fig. 8(c). By controlling the length of the left/right loading ends, $L_L$, $\omega_3$ can be tuned, as shown in Fig. 9(b).

Fig. 10 shows an optical microscope image of the fabricated device for characterization. The Ti/Au metal patterns were delineated with a standard optical lithography process followed by a lift-off process on top of a 300-$\mu$m thick quartz substrate. The dimensions of the fabricated device are slightly different from the mask layout with the dimensions shown in Fig. 1 due to the imperfect fabrication process. The devices exhibit approximately 1% fabrication error in dimensions and rounded corners instead of right angles.

The fabricated device was characterized using a commercial THz time-domain spectroscopy (TDS) system (TPS 3000) based on linearly polarized photoconductive antennas [47]. The measurements were carried out in a $N_2$ atmosphere to avoid the effect of water vapor in air.

Fig. 11(a) shows the measured transmittance of the fabricated device. The performance of self-complementary metasurface is compared with previously reported metasurfaces in Table 1. In this work, the three resonance frequencies for the x-polarized incident wave are almost the same as those for the y-polarized wave, and complementary spectral responses are achieved. Furthermore, the measured transmittance shows high polarization purity. The polarization extinction ratios (PERs), the ratios of the desired polarization component to the undesired component ($PER = 10log(P_{wanted}/P_{unwanted})$), are 18 dB, 24 dB and 18 dB at $\omega_1$, $\omega_2$ and $\omega_3$, respectively. The insertion losses are 0.17 dB, 0.46 dB and 0.69 dB at $\omega_1$, $\omega_2$ and $\omega_3$, respectively. The fractional bandwidths are 33, 21 and 19% at $\omega_1$, $\omega_2$ and $\omega_3$, respectively. Fig. 11(b) shows the measured phase responses. The phase difference of the two orthogonally polarized waves ranges from $-73°$ to $83°$ within a broad frequency range.

The simulation and measurement results are in fairly good agreement at the resonance frequencies, but the loss properties show 5.9% and 9.8% error at $\omega_2$ and $\omega_3$, respectively. The difference in the measurement and simulation results can be ascribed to the nonuniform dimensions as well as the line edge roughness of the fabricated metal patterns caused by the fabrication error inevitable in the contact aligner-based optical lithography and lift-off processes. Although the measured loss performance is quite good, it can be further improved by adopting more precise fabrication processes.

## IV. CONCLUSION

A multiband THz filter based on a self-complementary metasurface was demonstrated. Using equivalent circuits and EM simulation, its operational principles are presented, and the dominant geometric parameters that determine the resonance frequencies are identified. The self-complementary structures make it possible to design a 2-in-1 THz filter whose function can be chosen between BPF and BSF depending on the incident polarization. In addition to the filtering function, the two transmitted orthogonally polarized waves exhibit phase differences ranging from $-73°$ to $83°$ within a broad frequency range.

## REFERENCES


[1] S. S. Dhillon, M. S. Vitiello, E. H. Linfield, A. G. Davies, M. C. Hoffmann, J. Booske, C. Paoloni, M. Gensch, P. Weightman, G. P. Williams, and E. Castro-Camus, "The 2017 terahertz science and technology roadmap," *J. Phys. D, Appl. Phys.*, vol. 50, no. 4, pp. 1–49, Jan. 2017.

[2] R. A. Lewis, "A review of terahertz sources," *J. Phys. D, Appl. Phys.*, vol. 47, pp. 1–11, Aug. 2014.

[3] P. H. Siegel, "Terahertz technology in biology and medicine," *IEEE Trans. Microw. Theory Techn.*, vol. 52, no. 10, pp. 2438–2447, Oct. 2004.

[4] W. L. Chan, J. Deibel, and D. M. Mittleman, "Imaging with terahertz radiation," *Rep. Progr. Phys.*, vol. 70, no. 8, pp. 1325–1379, Jul. 2007.

[5] N. Nagai, T. Imai, R. Fukasawa, K. Kato, and K. Yamauchi, "Analysis of the intermolecular interaction of nanocomposites by THz spectroscopy," *Appl. Phys. Lett.*, vol. 85, no. 18, pp. 4010–4012, Nov. 2004.

[6] Z. Chen, X. Ma, B. Zhang, Y. X. Zhang, Z. Niu, N. Kuang, W. Chen, L. Li, and S. Li, "A survey on terahertz communications," *China Commun.*, vol. 16, no. 2, pp. 1–35, Feb. 2019.

[7] T. Nagatsuma, G. Ducournau, and C. C. Renaud, "Advances in terahertz communications accelerated by photonics," *Nature Photon.*, vol. 10, no. 6, pp. 371–379, May 2016.

[8] J. Y. Suen, "Terabit-per-Second satellite links: A path toward ubiquitous terahertz communication," *J. Infr., Millim., THz Waves*, vol. 37, no. 7, pp. 615–639, Jul. 2016.

[9] T. Kürner and S. Priebe, "Towards THz communications–status in research, standardization and regulation," *J. Infr., Millim., THz Waves*, vol. 35, no. 1, pp. 53–62, Aug. 2013.

[10] P. U. Jepsen, D. G. Cooke, and M. Koch, "Terahertz spectroscopy and imaging–modern techniques and applications," *Laser Photon. Rev.*, vol. 5, no. 1, pp. 124–166, Jan. 2011.

[11] S. B. Glybovski, S. A. Tretyakov, P. A. Belov, Y. S. Kivshar, and C. R. Simovski, "Metasurfaces: From microwaves to visible," *Phys. Rep.*, vol. 634, pp. 1–72, May 2016.

[12] B. Reinhard, O. Paul, and M. Rahm, "Metamaterial-based photonic devices for terahertz technology," *IEEE J. Sel. Topics Quantum Electron.*, vol. 19, no. 1, Jan. 2013, Art. no. 8500912.
[13] H. Zou and Y. Cheng, "Design of a six-band terahertz metamaterial absorber for temperature sensing application," *Opt. Mater.*, vol. 88, pp. 674–679, Feb. 2019.
[14] M. Kenney, J. Grant, and D. R. S. Cumming, "Alignment-insensitive bilayer THz metasurface absorbers exceeding 100% bandwidth," *Opt. Express*, vol. 27, no. 15, pp. 20886–20900, Jul. 2019.
[15] A. Nilotpal, S. Bhattacharya and P. Chakrabarti, "Frequency-and time-domain analyses of multiple reflections and interference phenomena in a metamaterial absorber," *J. Opt. Soc. Amer. B, Opt. Phys.*, vol. 37, no. 3, pp. 586–592, Mar. 2020.
[16] Nilotpal, L. Nama, S. Bhattacharyya, and P. Chakrabarti, "A metasurface-based broadband quasi nondispersive cross polarization converter for far infrared region," *Int. J. RF Microw. Comput.-Aided Eng.*, vol. 29, no. 10, pp. 1–9, Jul. 2019.
[17] J. Fan and Y. Cheng, "Broadband high-efficiency cross-polarization conversion and multi-functional wavefront manipulation based on chiral structure metasurface for terahertz wave," *J. Phys. D, Appl. Phys.*, vol. 53, no. 2, Jan. 2020, Art. no. 025109.
[18] N. Hussain and I. Park, "Design of a wide-gain-bandwidth metasurface antenna at terahertz frequency," *AIP Adv.*, vol. 7, no. 5, May 2017, Art. no. 055313.
[19] D. Wang, L. Zhang, Y. Gu, M. Q. Mehmood, Y. Gong, A. Srivastava, L. Jian, T. Venkatesan, C.-W. Qiu, and M. Hong, "Switchable ultrathin quarter-wave plate in terahertz using active phase-change metasurface," *Sci. Rep.*, vol. 5, no. 1, p. 15020, Dec. 2015.
[20] H.-T. Chen, W. J. Padilla, J. M. O. Zide, A. C. Gossard, A. J. Taylor, and R. D. Averitt, "Active terahertz metamaterial devices," *Nature*, vol. 444, no. 7119, pp. 597–600, Nov. 2006.
[21] M. T. Nouman, H.-W. Kim, J. M. Woo, J. H. Hwang, D. Kim, and J.-H. Jang, "Terahertz modulator based on metamaterials integrated with metal-semiconductor-metal varactors," *Sci. Rep.*, vol. 6, no. 1, p. 26452, May 2016.
[22] Y. Zhang, S. Qiao, S. Liang, Z. Wu, Z. Yang, Z. Feng, H. Sun, Y. Zhou, L. Sun, Z. Chen, X. Zou, B. Zhang, J. Hu, S. Li, Q. Chen, L. Li, G. Xu, Y. Zhao, and S. Liu, "Gbps terahertz external modulator based on a composite metamaterial with a double-channel heterostructure," *Nano Lett.*, vol. 15, no. 5, pp. 3501–3506, May 2015.
[23] H.-T. Chen, J. F. O'Hara, A. J. Taylor, R. D. Averitt, C. Highstrete, M. Lee, and W. J. Padilla, "Complementary planar terahertz metamaterials," *Opt. Express*, vol. 15, no. 3, pp. 1084–1095, Jan. 2007.
[24] D. Kim, S.-H. Eo, S.-I. Oh, and J.-H. Jang, "Spurious resonance suppression for a THz single bandpass filter using lossy glass substrates," *Microw. Opt. Technol. Lett.*, vol. 57, no. 1, pp. 58–60, Jan. 2015.
[25] J. M. Woo, D. Kim, S. Hussain, and J. H. Jang, "Low-loss flexible bilayer metamaterials in THz regime," *Opt. Express*, vol. 22, no. 3, pp. 2289–2298, 2014.
[26] J. M. Woo, D.-S. Kim, D.-J. Kim, and J.-H. Jang, "Terahertz filter integrated with a subwavelength structured antireflection coating," *AIP Adv.*, vol. 5, no. 12, Dec. 2015, Art. no. 127238.
[27] W. Withayachumnankul, B. M. Fischer, and D. Abbott, "Quarter-wavelength multilayer interference filter for terahertz waves," *Opt. Commun.*, vol. 281, no. 9, pp. 2374–2379, May 2008.
[28] C.-C. Chang, L. Huang, J. Nogan, and H.-T. Chen, "Invited article: Narrowband terahertz bandpass filters employing stacked bilayer metasurface antireflection structures," *APL Photon.*, vol. 3, no. 5, May 2018, Art. no. 051602.
[29] O. Paul, R. Beigang, and M. Rahm, "Highly selective terahertz bandpass filters based on trapped mode excitation," *Opt. Express*, vol. 17, no. 21, pp. 18590–18595, Oct. 2009.
[30] M. Khodaee, M. Banakermani, and H. Baghban, "GaN-based metamaterial terahertz bandpass filter design: Tunability and ultra-broad passband attainment," *Appl. Opt.*, vol. 54, no. 29, pp. 8617–8624, Oct. 2015.
[31] Y. Yuan, C. Bingham, T. Tyler, S. Palit, T. H. Hand, W. J. Padilla, D. R. Smith, N. M. Jokerst, and S. A. Cummer, "Dual-band planar electric metamaterial in the terahertz regime," *Opt. Express*, vol. 16, no. 13, pp. 9746–9752, Jun. 2008.
[32] L. Huang, C.-C. Chang, B. Zeng, J. Nogan, S.-N. Luo, A. J. Taylor, A. K. Azad, and H.-T. Chen, "Bilayer metasurfaces for dual-and broadband optical antireflection," *ACS Photon.*, vol. 4, no. 9, pp. 2111–2116, Aug. 2017.
[33] Y.-J. Chiang, C.-S. Yang, Y.-H. Yang, C.-L. Pan, and T.-J. Yen, "An ultra-broad terahertz bandpass filter based on multiple-resonance excitation of a composite metamaterial," *Appl. Phys. Lett.*, vol. 99, no. 19, Nov. 2011, Art. no. 191909.
[34] Y. Zhu, S. Vegesna, Y. Zhao, V. Kuryatkov, M. Holtz, Z. Fan, M. Saed, and A. A. Bernussi, "Tunable dual-band terahertz metamaterial bandpass filters," *Opt. Lett.*, vol. 38, no. 14, pp. 2382–2384, Jul. 2013.
[35] M. T. Nouman, J. H. Hwang, M. Faiyaz, K. J. Lee, D. Y. Noh, and J. H. Jang, "Vanadium dioxide based frequency tunable metasurface filters for realizing reconfigurable terahertz optical phase and polarization control," *Opt. Express*, vol. 26, no. 10, pp. 29–12922, May 2018.
[36] J. D. Ortiz, J. D. Baena, R. Marques, and F. Medina, "A band-pass/stop filter made of SRRs and C-SRRs," in *Proc. IEEE Int. Symp. Antennas Propag. (APSURSI)*, Spokane, WA, USA, Jul. 2011, pp. 2669–2672.
[37] J. D. Ortiz, J. D. Baena, V. Losada, F. Medina, R. Marques, and J. L. A. Quijano, "Self-complementary metasurface for designing narrow band pass/stop filters," *IEEE Microw. Wireless Compon. Lett.*, vol. 23, no. 6, pp. 291–293, Jun. 2013.
[38] J. D. Baena, J. P. del Risco, A. P. Slobozhanyuk, S. B. Glybovski, and P. A. Belov, "Self-complementary metasurfaces for linear-to-circular polarization conversion," *Phys. Rev. B, Condens. Matter*, vol. 92, no. 24, Dec. 2015, Art. no. 245413.
[39] J. A. Arnaud and F. A. Pelow, "Resonant-grid quasi-optical diplexers," *Bell Syst. Tech. J.*, vol. 54, no. 2, pp. 263–283, Feb. 1975.
[40] A. S. Arezoomand, F. B. Zarrabi, S. Heydari, and N. P. Gandji, "Independent polarization and multi-band THz absorber base on jerusalem cross," *Opt. Commun.*, vol. 352, pp. 121–126, Oct. 2015.
[41] S. Kundu, "Gain augmentation of a CPW fed printed miniature UWB antenna using frequency selective surface," *Microw. Opt. Technol. Lett.*, vol. 60, no. 7, pp. 1820–1826, May 2018.
[42] F. Costa, A. Monorchio, and G. Manara, "An overview of equivalent circuit modeling techniques of frequency selective surfaces and metasurfaces," *Appl. Comput. Electromagn. Soc. J.*, vol. 29, no. 12, pp. 960–976, Dec. 2014.
[43] F. Costa, A. Monorchio, and G. Manara, "Efficient analysis of frequency-selective surfaces by a simple equivalent-circuit model," *IEEE Antennas Propag. Mag.*, vol. 54, no. 4, pp. 35–48, Aug. 2012.
[44] X.-D. Hu, X.-L. Zhou, L.-S. Wu, L. Zhou, and W.-Y. Yin, "A miniaturized dual-band frequency selective surface (FSS) with closed loop and its complementary pattern," *IEEE Antennas Wireless Propag. Lett.*, vol. 8, pp. 1374–1377, 2009.
[45] S. Ghosh and K. V. Srivastava, "An equivalent circuit model of FSS-based metamaterial absorber using coupled line theory," *IEEE Antennas Wireless Propag. Lett.*, vol. 14, pp. 511–514, 2015.
[46] A. Ordal, R. J. Bell, R. W. Alexander, L. L. Long, and M. R. Querry, "Optical properties of fourteen metals in the infrared and far infrared: Al, Co, Cu, Au, Fe, Pb, Mo, Ni, Pd, Pt, Ag, Ti, V, and W," *Appl. Opt.*, vol. 24, no. 24, pp. 4493–4499, Dec. 1985.
[47] M. T. Nouman, J. H. Hwang, and J.-H. Jang, "Ultrathin terahertz quarter-wave plate based on split ring resonator and wire grating hybrid metasurface," *Sci. Rep.*, vol. 6, no. 1, p. 39062, Dec. 2016.

**SE-MI KIM** (Associate Member, IEEE) received the B.S. degree in electronics engineering from Konkuk University, Seoul, South Korea, in 2011, and the M.S. degree from the School of Information and Mechatronics, GIST, Gwangju, South Korea, in 2013, where she is currently pursuing the Ph.D. degree. Her research interests include THz sources, THz spectrometers, and metamaterial devices.

**CELSO M. LEITE** received the B.S. degree in electronics engineering from the Universidade Federal de Santa Catarina, Brazil, in 2017, and the M.S. degree from the School of Electrical Engineering and Computer Science, Gwangju Institute of Science and Technology (GIST), Gwangju, South Korea, in 2019. He is currently with Samsung Electronics. His research interests include tunable microwave devices and terahertz metamaterials.

**JU-YEONG PARK** received the B.S. degree in electrical engineering and computer science from the Gwangju Institute of Science and Technology (GIST), Gwangju, South Korea, in 2019, where he is currently pursuing the Ph.D. degree. His research interest includes GaN-based high-electron-mobility transistors (HEMTs).

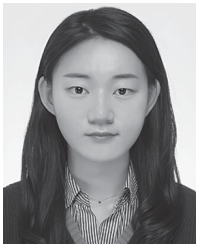

**HYO-JEONG KIM** received the B.S. degree from the School of Electrical Engineering and Computer Science, Gwangju Institute of Science and Technology (GIST), Gwangju, South Korea, in 2019. She is currently with LG Display. Her research interests include tunable microwave devices and terahertz metamaterials.

**JAE-HYUNG JANG** (Member, IEEE) received the B.S. and M.S. degrees in electrical engineering from Seoul National University, in 1993 and 1995, respectively, and the Ph.D. degree in electrical and computer engineering from the University of Illinois at Urbana–Champaign (UIUC) in 2002. He was a Research Associate with the Micro and Nanotechnology Laboratory, UIUC. He joined the Gwangju Institute of Science and Technology (GIST) in 2004, where he is affiliated with the School of Electrical Engineering and Computer Science as a Professor and the School Head. He also served as the Director of the Research Institute of Solar and Sustainable Energies (RISE). His research interests at GIST include InP- and GaN-based high-electron-mobility transistors (HEMTs), oxide semiconductor-based transparent thin-film transistors, and GaAs- and CIGS-based thin film solar cells. He is also conducting active research studies on active metamaterial devices based on compound semiconductor electronic devices for microwave and THz applications.